

Geophysical Research Letters

RESEARCH LETTER

10.1029/2019GL085639

Key Points:

- The STEVE comprises two traces, one at higher elevation and the other at lower elevation angle, due to their difference in emission height
- Both STEVE traces contain airglow continuum enhancement, but only the higher-elevation STEVE contains substantial red-line intensification
- We evaluate that the higher-elevation STEVE centers at ~250-km height, while the lower-elevation STEVE centers at ≤ 150 -km altitude

Supporting Information:

- Supporting Information S1
- Figure S1
- Figure S2

Correspondence to:

J. Liang,
liangj@ucalgary.ca

Citation:

Liang, J., Donovan, E., Connors, M., Gillies, D., St-Maurice, J. P., Jackel, B., et al. (2019). Optical spectra and emission altitudes of double-layer STEVE: A case study. *Geophysical Research Letters*, 46, 13,630–13,639. <https://doi.org/10.1029/2019GL085639>







Received 1 OCT 2019

Accepted 27 NOV 2019

Accepted article online 3 DEC 2019

Published online 10 DEC 2019

Optical Spectra and Emission Altitudes of Double-Layer STEVE: A Case Study

Jun Liang¹ , E. Donovan¹, M. Connors² , D. Gillies¹, J. P. St-Maurice³, B. Jackel¹ , B. Gallardo-Lacourt⁴ , E. Spanswick¹ , and X. Chu⁵ 

¹Department of Physics and Astronomy, University of Calgary, Calgary, Alberta, Canada, ²Athabasca University Observatories, Athabasca, Alberta, Canada, ³Department of Physics, University of Saskatchewan, Saskatoon, Saskatchewan, Canada, ⁴NASA/GSFC, Greenbelt, MD, USA, ⁵LASP, University of Colorado Boulder, Boulder, CO, USA

Abstract We report an event study of STEVE on 17 July 2018, with focus on the optical spectra and emission altitudes of STEVE. We find that the STEVE comprises two traces, one at a higher elevation angle and the other at a lower elevation angle. The two traces merge into one when viewed near the zenith. Spectrograph measurements show that both STEVE traces are characterized by enhancements over broadband wavelengths, that is, an airglow continuum, but they differ in their red-line (630 nm) component: The higher-elevation STEVE contains substantial red-line enhancement over background, while the lower-elevation STEVE does not. Based upon triangulation analyses using multiple optical instruments, we evaluate that the two STEVE traces are likely emitted from distinctly different altitudes: The higher-elevation STEVE comes from ~250-km altitude, while the lower-elevation one is from ≤ 150 -km altitude. Our results impose implications and constraints on the possible underlying mechanisms of STEVE.

Plain Language Summary The recently discovered STEVE nightglow is active at times of auroral activity but does not seem to be an aurora. It is located at lower latitudes than the usual aurora, and as photographed on the citizen science cameras which played a large role in drawing attention to it, it has a different color. In this study, using a combination of scientific optical instruments, especially the spectrograph recently deployed at Lucky Lake, Canada, by the University of Calgary, we investigate the optical spectral properties of STEVE and their emission altitudes. Two major spectral (color) components of STEVE are identified. One is characterized by a broadband enhancement over the entire visible wavelength range, contributing to the apparently “whitish” color of the STEVE, and the other is contributed by oxygen airglow concentrated at 630 nm, adding a “reddish” tint to the STEVE. In the event occurring on 17 July 2018, the STEVE is found to comprise two emission structures originating from different altitudes, one at ~250 km and the other at ≤ 150 -km altitude. Both STEVE structures contain the white component but only the higher-altitude one shows a substantial red component. That red color is the same red as seen in auroras that come from high altitudes in the atmosphere, while the mechanism of the white component remains to be explored.

1. Introduction

STEVE is a night sky optical phenomenon initially discovered by citizen scientists and auroral photography enthusiasts and then received keen interest by the space physics community. To date, while its generation mechanism remains unknown, two key properties of STEVE have gained wide consensus. (a) STEVE is located equatorward of traditional auroras, and there has been no evidence of appreciable electron/proton precipitation that could be the cause of the luminosity (Gallardo-Lacourt et al., 2018; Gallardo-Lacourt et al., 2018; MacDonald et al., 2018), suggesting that STEVE is not traditional aurora. (b) STEVE was found to be colocated with strong ionospheric electron heating and fast subauroral ion drifts in joint optical and in situ satellite observations (Archer et al., 2019; Chu et al., 2019; Macdonald et al., 2018; Nishimura et al., 2019). These findings lead to the retagging of STEVE as “Strong Thermal Emission Velocity Enhancement” (MacDonald et al., 2018). This has become the accepted scientific name of the phenomenon.

Recently, Gillies et al. (2019) reported an important finding based upon spectrograph measurements: STEVE contains an overall enhancement of a continuous spectrum spanning between ~400 and 730 nm as its main

source of brightness. While the existence of night airglow continuum (AGC) has been known for decades (e.g., Barbier et al., 1951), their commonly reported AGC intensities in the existing literature (e.g., Sternberg & Ingham, 1972) are much weaker than that of STEVE (Gillies et al., 2019; and the fact that STEVE is visible to the naked eyes). So far, the generation mechanism of the STEVE AGC and the underlying magnetosphere-ionosphere-thermosphere coupling processes have remained elusive.

A key point in finding an explanation for what happens in STEVE is to determine its emission altitudes. The ionosphere and thermosphere are highly altitudinally variable. Chemical and physical processes differ substantially at different height ranges. Optical emissions, either auroras or airglows, are known to have different altitudinal dependences at different wavelengths (colors). The emission altitude would thus offer key clues to and impose constraints on the possible mechanism(s) of STEVE. To the authors' knowledge, there are a few existing attempts to use the citizen scientists' photographs to evaluate the STEVE emission altitudes, and such an approach will also be included in this study. For example, in a case study Archer et al. (2019) estimated the altitude range of STEVE to be within ~130–270 km, with a clear distinction between a “mauve” STEVE at higher altitudes and a more “whitish” STEVE at lower altitudes. However, it is incontrovertible that well-calibrated scientific instruments are generally advantageous in narrowing down the uncertainty of positioning and yielding more accurate results. In this letter, we shall use multi-station optical instruments to investigate the spectra and emission altitudes of the internal structure of STEVE and tentatively discuss the implication of our findings to the possible generation mechanism of STEVE.

2. Observations

The STEVE event of interest occurred on 17 July 2018. Major optical instruments used in this study include the multiwavelength all-sky-imagers (ASIs) of the Athabasca University Geophysical Observatory (AUGSO) at Athabasca (54.60°N, 113.64°W), the Redline Emission Geospace Observatory (REGO), the Four-Eight-Six-One (FESO) photometer and the Transition Region Explorer Spectrograph (TRSp). REGO/TRSp/FESO are collocated at Lucky Lake (LUCK, 51.15°N, 107.26°W). REGO is a 630-nm red-line imager (Liang et al., 2016). FESO is a meridian-scanning photometer designed for H_β proton auroras (Unick et al., 2017) but is used in this study as a proxy of AGC. TRSp is an imaging spectrograph designed to yield the optical spectra between ~400 and 800 nm of night sky emissions at 0.4-nm resolution along a geographical meridian (Gillies et al., 2019). AUGSO runs in 30- to 60-s cadence depending on the wavelength, while the time resolution of REGO/TRSp/FESO is 3 s/15 s/30 s, respectively.

2.1. Observational Geometry and Optical Features of Interest

Figure 1 serves to display the observational geometry and to give a snapshot demonstration of all optical features of interest in this study. Figure 1a displays a combined 630-nm image map of AUGSO and REGO (raw images shown on the leftside), assuming an emission altitude of 247 km, with the scan meridian lines of FESO (blue) and TRSp (white) overplotted. Near the northern edge of the images there are some auroras. Equatorward of the auroras, REGO and AUGSO 630 nm images show two arcs. The more poleward brighter one represents the STEVE of interest, which was newly intensified after 0642 UT. RBSP-B satellite crosses the magnetospheric footprint of this STEVE at ~0647 UT, when strong subauroral ion drift flows are found (Chu et al., 2019). It is important to note that this STEVE is prominently shown on all available AUGSO wavelengths, including 620 and 480 nm (Figures 1b and 1d), which are not characteristic of any major auroral/airglow emissions and are actually designed for background subtraction for neighboring auroral lines (630 and 486.1 nm). This observation offers evidence of the AGC nature of STEVE (Gillies et al., 2019). To evaluate the STEVE emission altitude, we first determine the center peak of the STEVE arc as well its half widths using a two-side Gaussian fit with a linear background in each image epoch. The best fit center emission altitude is determined according to the height that best matches the arc center (shown as dashed line in Figure 1a) viewed by two imagers, which is 247 km in this frame. The uncertainty range of the center emission altitude is evaluated according to the height with which the STEVE arc center in AUGSO matches the lower (higher) half-width boundary of the arc in REGO, which is found as 232 km (260 km) here. In addition to STEVE, there is one other broader arc to the south of STEVE on both AUGSO and REGO 630-nm images. This southern arc has been preexisting and can be traced back to ~0550 UT on REGO, well before the emergence of STEVE; it represents a stable auroral red-line (SAR) arc (Rees & Roble, 1975). This SAR arc is solely seen in 630 nm but not in other wavelengths, in contrast to the broad spectral property of

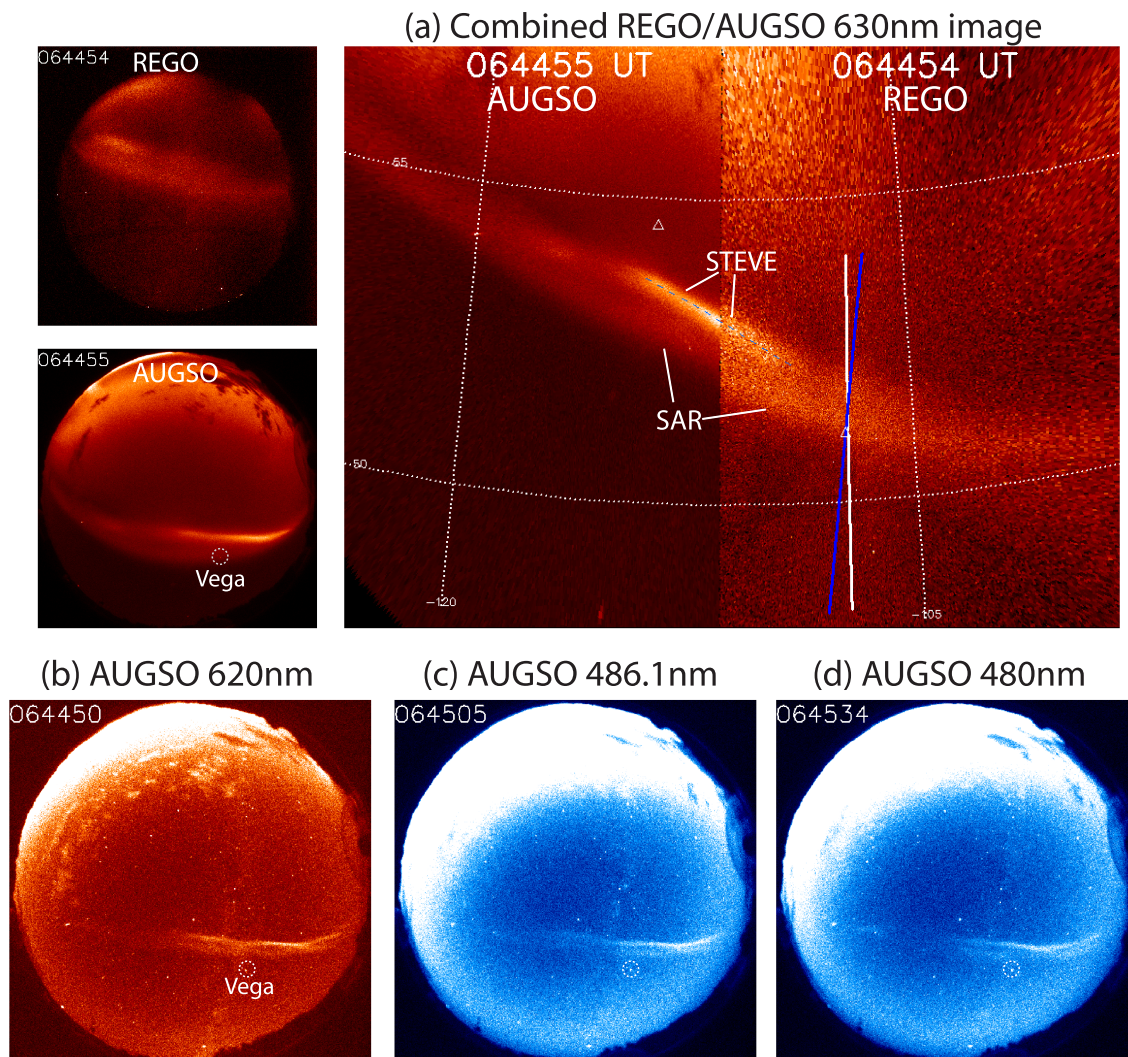


Figure 1. (a) A combined 630-nm image of AUGSO and REGO in geographical coordinates, with the scan meridians of FESO (blue) and TRSp (white) overplotted. Raw images of the two ASI ae also given on the leftside. An emission altitude of 247 km is assumed. The two triangles indicate the center of the AUGSO (more poleward) and REGO (more equatorward) ASIs. (b–d) AUGSO 620-, 486.1-, and 480-nm raw images. In all AUGSO raw images, Vega is marked to facilitate distinguishing SAR and STEVE

STEVE. In the following subsections we shall further elucidate the difference between the optical spectral properties of SAR and STEVE using TRSp data. In passing we note that the SAR seems not to match in latitudes on two imagers in Figure 1a, since the applied altitudes (247 km) here is intended to match the STEVE—an altitude of ~300 km would be more appropriate to match the SAR on two imagers (not shown). One other subtlety that can be viewed from Figures 1b to 1d is that upon a close look there are two separate arcs, of which the higher-elevation one (closer to the image center) is stronger and corresponds to the STEVE arc on the 630 nm image, while there is no discernible counterpart of the weak lower-elevation arc on the 630 nm image—one should not confuse the 630-nm SAR with the lower-elevation STEVE, as can be readily checked with their relative location with stars (Vega is marked) in the AUGSO FoV.

2.2. REGO/FESO/TRSp Observations of STEVE: Double Traces

While the initial appearance of STEVE is from ~0630 UT, before 0642 UT the STEVE was mainly recorded by AUGSO (see Figures 3g and 3h later for examples). By that time, the STEVE shows variable azimuthal

extension and sometimes reaches the LUCK meridian, producing some intermittent signatures on FESO/TRSp there, but no well-defined STEVE structure is seen on REGO 630 nm images before ~0642 UT. After ~0642 UT, a new STEVE arc begins to intensify and grow in the REGO FoV, poleward of the preexisting SAR. The top panel of Figure 2a shows the keogram of REGO 630-nm images sampled along the FESO meridian at LUCK. Readers are referred to the supplementary movie to view the full evolution. The newly intensified STEVE gradually moves southward, eventually merging with and replacing the preexisting SAR. The second panel shows the FESO data in its background channel (average of two 3-nm bands at 480 and 495 nm). Noticeable southward moving traces of emission structures can be identified. We have also checked the signal channel (486.1 nm) of FESO and confirmed that identical traces are seen and that the true proton auroral intensity (background subtracted) is essentially zero. These traces thus do not represent proton aurora—they actually lie distinctly equatorward of proton auroras—but indicate the AGC enhancement contained in STEVE (see also Figures 1c and 1d). The bottom panel of Figure 2a shows the AGC intensity obtained from TRSp. Throughout this letter, the AGC intensity on TRSp is defined as the integrated spectrum over the wavelength range 420–720 nm, excluding 423–430, 555–560.5, and 627–639.5 nm bands to remove contributions from prominent discrete aurora/airglow emission lines at 427.8, 557.7, and the 630–636.4 nm doublet. In short, the top panel of Figure 2a shows the OI 630-nm emission line component, while the other two panels represent the AGC component. Similar southward-moving traces of AGC enhancements, that is, STEVE, can also be seen on TRSp.

Upon inspection of the STEVE traces in FESO/TRSp data, one can notice a separation between higher-elevation and lower-elevation traces. Some of these traces at times appear to be weak and intermittent. This may be due to the variability of the azimuthal extension (e.g., whether the STEVE reaches the FESO/TRSp meridian) and/or small-scale spatiotemporal fluctuations of the STEVE, which we indeed notice from AUGSO/REGO data but shall not pursue in detail in this letter. The motion of the two traces closely follows each other, and they appear to merge into one at ~0710 UT as they pass the zenith. Prior to ~0640 UT, the lower-elevation trace is stronger, while after 0642 UT the higher-elevation trace becomes stronger. This latter higher-elevation trace corresponds to the STEVE arc seen on REGO, except that the REGO STEVE features a slightly broader elevation span than the AGC component of the STEVE seen on FESO/TRSp, presumably owing to the long radiative lifetime nature of the 630-nm emission. In contrast, throughout the entire event interval the lower-elevation STEVE trace has no discernible counterpart on REGO. We also note that the SAR is solely seen on REGO 630 nm, with no imprint on AGC. These observations indicate that SAR and STEVE are different optical phenomena that are spatially and spectrally discrepant.

The existence of such double traces of STEVE is also present in AUGSO 620/480 nm observations. One example has been given and addressed in Figures 1b–1d. In the supporting information (Figure S1), we display a series of AUGSO 620-nm images together with concurrent 630-nm images, to demonstrate the configuration and temporal evolution of the double-arc STEVE structure. In short, the stronger higher-elevation arc seen on 620-nm images is the counterpart of the STEVE seen on 630-nm images, while the weak lower-elevation STEVE arc seen on 620-nm images is not discernible on 630-nm images. The double-layer STEVE is also captured in photos from a citizen scientist (Neil Zeller; see Figure S2 in the supporting information).

In principle, a separation in elevation angles viewed by a ground imager may be caused by either a mainly horizontal or a mainly altitudinal difference of emissions. In our event, combined observations from AUGSO and FESO/TRSp offer a special clue to resolve the above ambiguity. Athabasca is located north of STEVE, while Lucky Lake is mostly south of STEVE. Since the stronger trace with 630-nm counterpart (weaker trace without 630-nm enhancement) is found at higher (lower) elevation angles as viewed from both stations after 0642 UT, the observation is more prone to be interpreted as altitudinally separated structures: a higher (lower) elevation angle indicates a higher (lower) emission height. The interpretation as altitudinal structures also helps explain two other notable facts in observations. (1) The lower-elevation trace contains no 630-nm emission enhancement, due to ineffective production and high collisional quenching rate of O (¹D) at lower altitudes (Solomon et al., 1988). (2) As seen on FESO/TRSp, the two traces closely follow each other in the course of their motion and appear to merge when they pass overhead of FESO/TRSp (the double-arc configuration is still seen on AUGSO by that time; see the last panel of Figure S1). They might not merge exactly at the zenith, since it is possible that the structure is not strictly vertical but slightly horizontally separated as well (see Figure 4a).

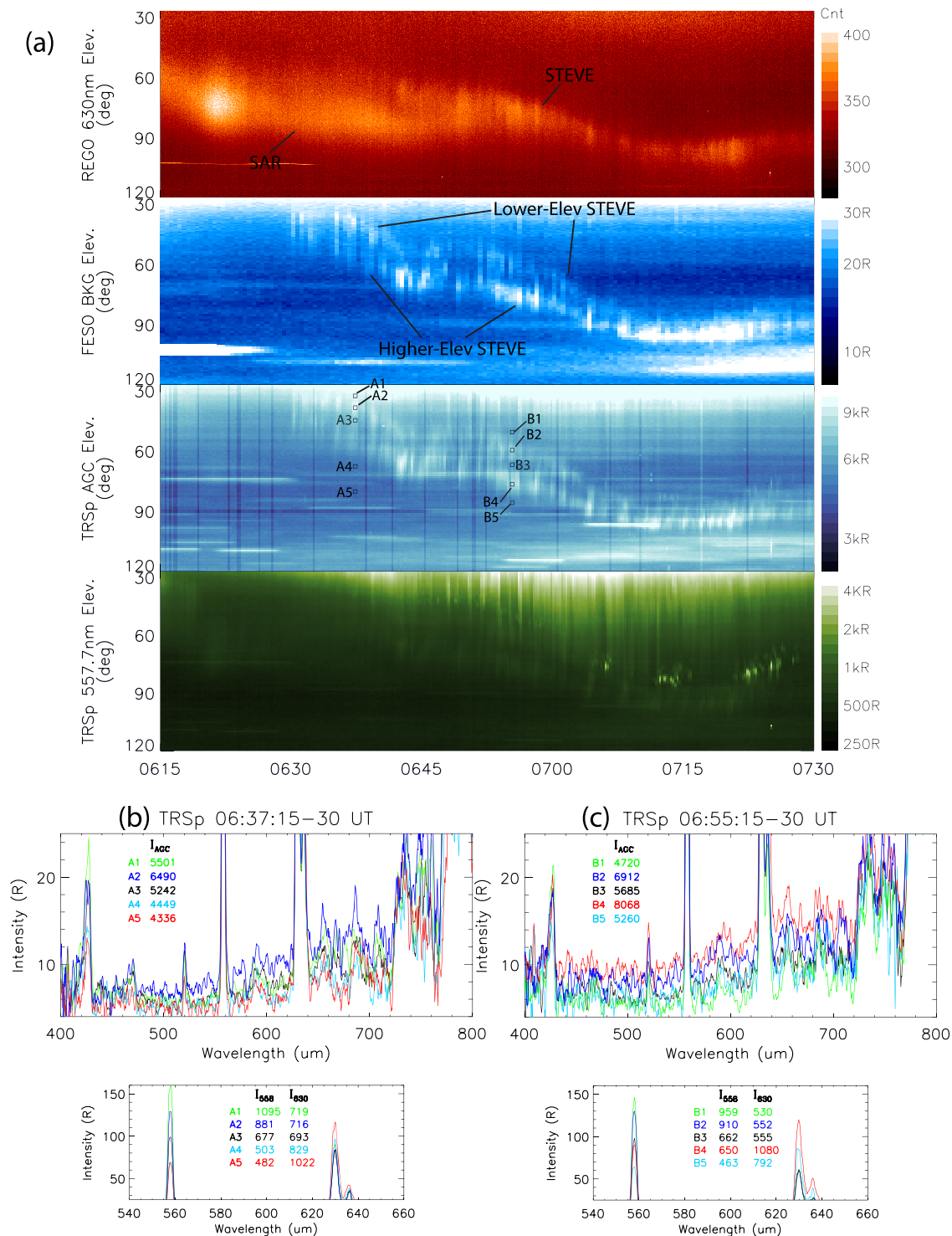


Figure 2. Top panel of (a) shows REGO 630 nm keogram sampled along the FESO meridian. The middle panel shows the keogram of FESO background channel intensity. The third panel and the bottom panel show the keograms of AGC intensity and green-line intensity, respectively, obtained from TRSp measurement. In all plots, the elevation angle is calculated from the northern horizon. Note that some of the bright strips (including those at $>100^\circ$ elevation) on FESO/TRSp are from stars/planets. The sample regions for spectral analyses are: A1/A3: STEVE neighboring background, A2: lower-elevation STEVE, A4: SAR background, A5: SAR; B1/B3/B5 lower/gap/higher background of STEVE, and B2/B4: lower/higher-elevation STEVE. (b and c) The sampled optical spectra. Their plot range and format are designed to focus separately on AGC and 557.7-/630.0-nm emission lines. Y axis indicates measured Rayleigh in each bin (to get R/nm, multiply by ~ 2.5). Raw spectral resolution (~ 0.4 nm) is used in the lower panel, while a five-bin sliding smooth is applied to the spectra in the upper panel. The total AGC, green-line and red-line intensities of all sampled phenomena (in unit of Rayleigh) are marked

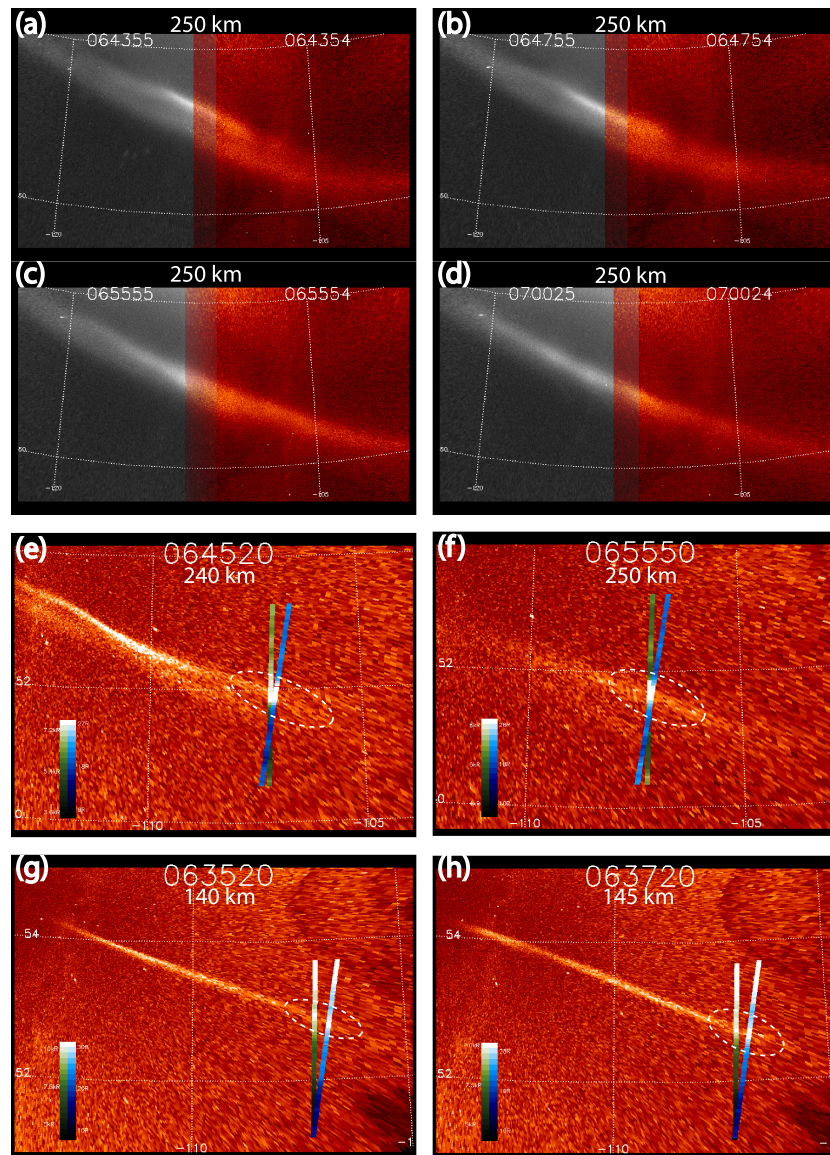


Figure 3. (a–d) Combined 630-nm red-line image of AUGSO (left) and REGO (right); an emission altitude of 250-km altitude is applied. Image time is labeled for each camera. The overlapping FoV of the two ASIs is presented as an alpha-blending overlay of two images. (e–h) AUGSO 620-nm images overplotted with TRSp & FESO AGC intensities; the emission altitude applied is labeled at the top of each subfigure

2.3. Spectral Characteristic of STEVEs

In this subsection, we exemplify the optical spectra of STEVEs and compare with their neighboring background. The sampling epochs and regions are labeled in the bottom panel of Figure 2a. More specifically, we collect the spectra that correspond to the earlier low-elevation STEVE and to the two later STEVE traces, as well as their surrounding neighbors. The earlier high-elevation trace, though marginally perceptible, is too weak and without distinguishable optical counterpart on ASIs, so that it is not studied here. For the earlier epoch we also sample the SAR (A5, according to REGO data) and its neighboring background (A4) for comparison, while for the later epoch we also include the gap (B3) between the lower- and higher-elevation STEVEs. See figure caption for all legend details. A van Rhijn correction (Best, 1965) is applied to the data to suppress the elevation angle bias. Figures 2b and 2c show the sampled spectra for the two epochs; their plot range and format are designed to focus separately on the AGC and on the 557.7-/630.0-nm emission lines.

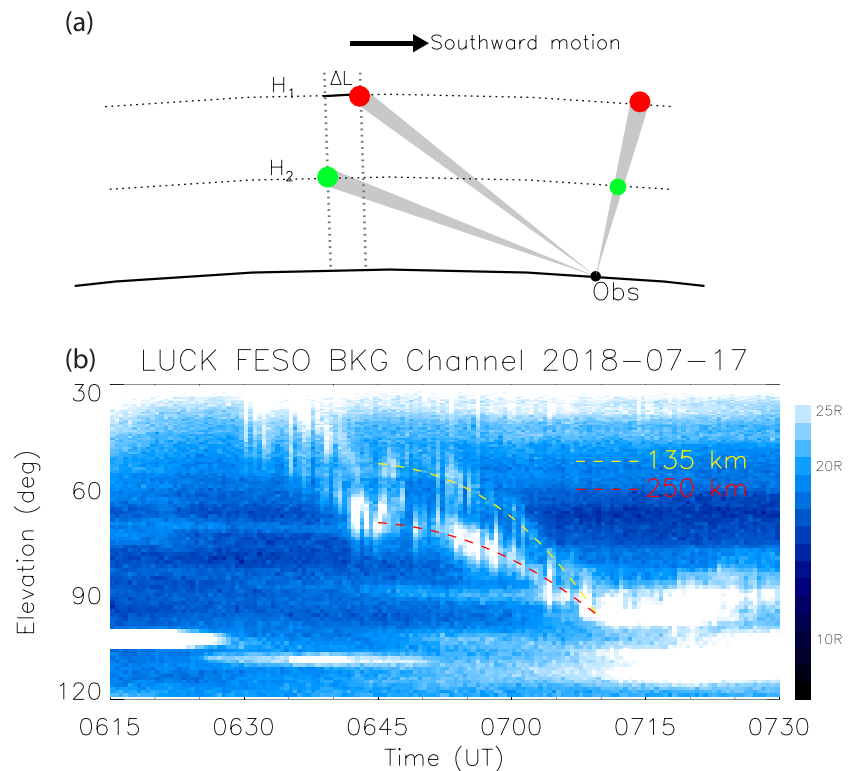


Figure 4. (a) A sketch plot showing the geometry applied in attempt to estimate the emission altitude of lower-elevation STEVE. Two cones originated from an observer denote the higher- and lower-elevation structures in our observation; they visually overlap when they are visually aligned with the observer. (b) FESO data at the background channel. A red dashed line shows the fitted location and motion of the observed high-elevation STEVE at 250-km altitude; a yellow dashed line shows the expected location and motion of a corresponding lower-altitude structure at 135-km altitude, which best fit the realistic observation of the lower-elevation STEVE trace

The total AGC intensity, green-line intensity (integrated over 555–560.5 nm) and red-line intensity (integrated over 627–633 nm) are given for each phenomenon. One can see that the spectra of all sampled STEVEs (A2, red curve in Figure 2b, and B2/B4, blue/red curves in Figure 2c) feature broadband enhancements above their neighboring background (A1/A3 and B1/B3/B5). This result confirms the finding in Gillies et al. (2019) that AGC constitutes the spectral characteristics of STEVE. In contrast, the SAR (A5, red curve in Figure 2b) contains strong 630-nm emissions yet no AGC enhancement. On the other hand, the higher-elevation STEVE (B4) in Figure 2c also contains an enhanced 630-nm emission component, while for the lower-elevation STEVE spectra (A2 and B2), the 630-nm intensity is found not to be pronouncedly different from their surrounding background, consistent with the fact that they are not discernible on REGO. To summarize, both higher- and lower-elevation STEVEs feature AGC enhancements, but they differ in 630 nm emission enhancement.

The bottom panel of Figure 2a shows the 557.7-nm keogram inferred from TRSp. Green line is usually the dominant emission in auroras but is minor only in STEVE luminosity. There is a feeble 557.7-nm trace that corresponds to the higher-elevation STEVE, but the associated intensity is much weaker than the AGC component—and part of the intensity may actually stem from the AGC enhancement over the green-line band. There is a consistent trend of increasing 557.7-nm intensity toward lower elevations, which is found to persist even after the van Rhijn correction. The green-line intensity contained in the lower-elevation STEVE is masked by such an ambient trend, so that its trace is not discernible in the 557.7-nm keogram. We, however, notice that some strong yet intermittent green-line emissions, often known as “picket-fence” (see the bottom panel of Figure 2a), appear to have roughly collocated AGC structures after 0707 UT, suggesting a possible link between the picket-fence and the lower-altitude AGC intensification, but a further exploration on this topic is beyond the content of the current paper.

2.4. Emission Altitude of STEVEs

We now evaluate the emission altitudes of STEVE using multi-station triangulation. We first perform the analyses on the strongest observed STEVE trace, that is, the higher-elevation STEVE after 0642 UT. This STEVE contains a strong red-line component that is seen on both REGO and AUGSO 630-nm imagers. The two ASIs constitute an ideal geometry for triangulation since the STEVE is situated amid the two ASI's overlapping FoV. Figures 3a–3d show a few combined images of AUGSO/REGO 630-nm images. The best fit center emission altitude for the STEVE is found to be fairly stable at ~250 km throughout the interval 0643–0710 UT. Two methods are used to estimate the altitude uncertainty. One is that described in section 2.1, and the other utilizes the fact that when approaching 0700 UT and after, the STEVE arc is fairly close to the REGO zenith. We may thus reasonably assume that the apparent arc broadness seen overhead by REGO represents the latitudinal width of the arc and estimate the altitudinal extension of emissions using oblique AUGSO observations. The above two methods yield compatible results; both unveil an altitudinal range within ~230–270 km.

Next, we examine the emission altitude of the AGC component of STEVE. We have checked and confirmed that the AUGSO 620-nm high-elevation STEVE essentially collocates with the 630-nm STEVE (see Figure S1). A direct evaluation of the AGC emission altitude can be made via triangulation between AUGSO 620-nm images and FESO/TRSp, though the geometry is slightly inferior to that with REGO since FESO/TRSp scan lines are near the eastern edge of the AUGSO FoV. Figures 3e and 3f display two examples of such an effort. By matching the AUGSO 620-nm higher-elevation STEVE and the strong AGC intensification structures seen on FESO/TRSp, a best fit altitude of ~240–250 km is achieved. Within the uncertainty of our procedures, it is reasonable to state that the AGC and the 630-nm components, two dominant constituents of the high-elevation STEVE brightness, feature similar emission altitudes centered around ~250 km.

We have also checked the emission altitude with the STEVE photographs taken by a citizen scientist, Colin Chatfield (see supporting information). We have found that the REGO/AUGSO observations and Chatfield's photos, if all projected to the same altitude of 250 km, yield consistent geometry between the STEVE and stars (see Figure S3). This lends further support for our derived emission altitude.

We then look into the emission altitude of the lower-elevation STEVE. We have also attempted triangulation between AUGSO 620-nm images and FESO/TRSp AGC structures for this purpose. Unfortunately, the lower-elevation STEVE after ~0642 UT is a bit weak and intermittent; it either does not extend to FESO/TRSp meridian, or its extension is too vague to be reliably discerned due to noise contamination at low elevation angles of AUGSO (e.g., see Figures 3e and 3f). That said, some reliable triangulation results can be achieved for certain earlier periods before 0640 UT when the lower-elevation STEVE is stronger on AUGSO with longer-stretched extension, though a possible time-varying effect of emission altitudes may not be studied under this approach. Figures 3g and 3h exemplify two such earlier AUGSO images overplotted with FESO/TRSp AGC intensities. By matching the strong AGC traces on these instruments, we derive a best fit emission altitude of 140–145 km.

One way to indirectly estimate the emission height of the lower-elevation STEVE is via the known emission height of the higher-elevation STEVE, upon a premise that the two traces are mainly altitudinally separated. Figure 4a shows the geometry applied to our approach. The two STEVEs are deemed to be separated by both an altitudinal offset $H = H_1 - H_2$ and a horizontal distance L , in which the former is dominant. We set the center emission height $H_1 = 250$ km for the higher-elevation STEVE according to the above triangulation result. We trace the motion of the center of the higher-elevation STEVE during 0645–0710 UT and fit it into a second-order polynomial as a function of time, as overplotted in Figure 4b in a red curve. It is difficult to unequivocally determine the horizontal separation L from available data. Nevertheless, inferred from the FESO/TRSp observation that only one single bright arc at ~96° elevation is seen after ~0710 UT, we postulate that the higher- and lower-elevation STEVEs visually overlap at such an angle, and assume $L \sim H \cdot \tan(6^\circ)$ as our best guess. While the lower-elevation STEVE is a bit weak and intermittent, according to available traces we are able to evaluate a best fit curve corresponding to $H_2 \sim 135$ km, which is overplotted in Figure 4b as a yellow curve. A choice of L within ~10–20 km would lead the best fit height to vary between ~125 and 150 km, while $L > 20$ km would cause a $> 5^\circ$ angular separation overhead which is not evident for STEVE after ~0710 UT. Note that we do not assume a magnetic field alignment of STEVE structures, considering the likelihood that the STEVE AGC stems from chemiluminescence in which neutral chemistry/dynamics are

crucially involved (see section 3). Though not without uncertainty, we estimate that the emission altitude of the lower-elevation STEVE is likely smaller than and/or close to 150 km. This is compatible with the triangulation result for the STEVE before 0640 UT as shown in Figures 3g and 3h.

3. Summary and Discussion

In this study, we corroborate the recent finding by Gillies et al. (2019) that STEVE features AGC enhancement as its main source of brightness. Furthermore, we find that the STEVE in this event comprises two traces, one at higher elevations and the other at lower elevation angles. The higher-elevation STEVE contains substantial 630-nm red-line intensification, while the lower-elevation STEVE does not. We suggest that the separation between the two traces are mainly due to their different emission altitudes. Using triangulation analyses with multi-station optical instruments, we derive a center emission altitude of ~250 km for the higher-elevation STEVE, while the lower-elevation STEVE likely comes from much lower emission altitudes (≤ 150 km). We footnote that we have also noticed double-layer structures with different “colors” in other STEVE events, from both scientific ASIs and citizen scientists’ photos. In such events, a more “pinkish” STEVE is viewed at higher elevation/altitude, while a more “whitish” STEVE would be situated at lower elevation/altitude (see, e.g., Figure S2 and Archer, St.- Maurice, et al., 2019).

A SAR arc is also observed in this event but is found to be distinctly different from the STEVE. Since the beginning of the STEVE research, there has been curiosity about the similarity between STEVE and SAR. Previous identification of STEVE was usually based upon white light or 630-nm red-line imagers, making it difficult to unequivocally discriminate SAR and STEVE phenomena. In this study, with TRSp observations of SAR and STEVE, we for the first time clearly demonstrate their fundamental discrepancy. They differ in spatial and temporal variations and, most crucially, in spectral characteristics: The SAR has no AGC enhancement component, while the lower-elevation STEVE has no 630-nm enhancement. It is the AGC enhancement that constitutes the unique characteristic of STEVE distinguishing itself from SAR. The STEVE AGC may also partly explain the result in Mende and Turner (2019). For example, for the blue component of STEVE in their color analyses, which they proposed as resulting from auroral $N_2^+ 1 N$ emissions, could be at least partly contributed by the AGC.

To date, two most common explanations of the AGC are the NO_2 continuum (e.g., Hedin et al., 2012; Sternberg & Ingham, 1972) via a radiative recombination reaction $NO+O \rightarrow NO_2+h\nu$ and certain meteoric metal-induced pseudo-continuum (e.g., Evans et al., 2010). Two outstanding issues of the existing AGC mechanisms are as follows: (a) They usually yielded optical intensities much lower than that of STEVE; (b) their excitation was often conceived to be confined in the lower thermosphere (<120 km) for the NO_2 continuum and even lower for the meteoric metal-involved AGC (<100 km). Our derived emission altitudes, particularly that of the higher-elevation STEVE (~250 km), impose challenges and new aspects to the above mechanisms. It is fair to state that the meteoric metal-involved AGC is invalidated as a major candidate of STEVE. Using the documented reaction rate of the NO_2 continuum (e.g., Hedin et al., 2012), we estimate that the $[NO][O]$ density product is required to be on the order of 10^{19} – 10^{20} cm^{-6} , to be capable of producing the observed STEVE brightness in this study and Gillies et al. (2019). Such densities are large even for the lower-altitude STEVE and, at first blush, seem unrealistic for the higher-altitude STEVE at ~250 km. We however noted that existing observations indicate that STEVE embodies extreme conditions in terms of ionospheric/thermospheric heating which is conducive to NO production in numerous ways and that unusual NO enhancement has indeed occasionally been reported in the literature. For example, Zipf et al. (1970) found in an event in which the $[NO][O]$ product exceeded 2×10^{21} cm^{-6} at 120-km height. Furthermore, the temperature dependence of reaction rates involved in AGC production remains poorly determined so far. Previous experiments of the NO_2 continuum reaction rate were mostly conducted in the lower thermosphere with $T \sim 200$ – 350 K, though the temperature dependence was tentatively studied in Sharp (1984) and Hedin et al. (2012). It is questionable that the documented NO_2 continuum rates be applicable to the upper thermosphere ($T \sim 1000$ K at 250 km). To proceed, realistic measurements of the density/temperature/speed of neutrals associated with STEVE, model simulations of STEVE-related magnetosphere-ionosphere-thermosphere processes with focus on the heating and neutral enhancement, and more accurate depiction of the reaction rates at high temperature are desirable research directions in the future for us to understand the STEVE AGC.

Acknowledgments

REGO and FESO are supported by the Canada Foundation for Innovation (CFI) and the Canadian Space Agency. AUGSO is supported by the CFI. REGO and FESO data are publicly available at <http://data.phys.ucalgary.ca> website. TReX is jointly funded by CFI, Alberta Economic Development and Trade, and the University of Calgary. TReX data will be fully open to public by early 2020. All TReX and AUGSO data used in this study are downloadable at http://data.phys.ucalgary.ca/sort_by_project/other/publication_datasets/2019GL085639/ website. We thank Shasha Zou, Y. Nishimura, and Wenbin Wang for their useful discussions.

References

- Archer, W. E., Gallardo-Lacourt, B., Perry, G. W., St.-Maurice, J. P., Buchert, S. C., & Donovan, E. (2019). Steve: The optical signature of intense subauroral ion drifts. *Geophysical Research Letters*, *46*, 6279–6286. <https://doi.org/10.1029/2019GL082687>
- Archer, W. E., St.-Maurice, J. P., Gallardo-Lacourt, B., Perry, G. W., Cully, C. M., Donovan, E., et al. (2019). The vertical distribution of the optical emissions of a Steve and Picket Fence event. *Geophysical Research Letters*, *46*, 10,719–10,725. <https://doi.org/10.1029/2019GL084473>
- Barbier, D., Dufay, J., & Williams, D. (1951). Recherches sur l'émission de la raie verte de la lumière du Ciel nocturne. *Annual Astrophysics*, *14*, 399–437.
- Best, G. T. (1965). A new use of the Van Rhijn formula for airglow measurements. *Planetary and Space Science*, *13*, 855–860.
- Chu, X., Malaspina, D., Gallardo-Lacourt, B., Liang, J., Andersson, L., Ma, Q., et al. (2019). Identifying STEVE's magnetospheric driver using conjugate observations in the magnetosphere and on the ground. *Geophysical Research Letters*, *46*. <https://doi.org/10.1029/2019GL082789>
- Evans, W. F. J., Gattinger, R. L., Slanger, T. G., Saran, D. V., Degenstein, D. A., & Llewellyn, E. J. (2010). Discovery of the FeO orange bands in the terrestrial night airglow spectrum obtained with OSIRIS on the Odin spacecraft. *Geophysical Research Letters*, *37*, L22105. <https://doi.org/10.1029/2010GL045310>
- Gallardo-Lacourt, B., Liang, J., Nishimura, Y., & Donovan, E. (2018). On the origin of STEVE: Particle precipitation or ionospheric skyglow? *Geophysical Research Letters*, *45*(16), 7968–7973. <https://doi.org/10.1029/2018GL078509>
- Gallardo-Lacourt, B., Nishimura, Y., Donovan, E., Gillies, D. M., Perry, G. W., Archer, W. E., et al. (2018). A statistical analysis of STEVE. *Journal of Geophysical Research: Space Physics*, *123*, 9893–9905. <https://doi.org/10.1029/2018JA025368>
- Gillies, D. M., Donovan, E., Hampton, D., Liang, J., Connors, M., Nishimura, Y., et al. (2019). First observations from the TReX spectrograph: The optical spectrum of STEVE and the picket fence phenomena. *Geophysical Research Letters*, *46*, 7207–7213. <https://doi.org/10.1029/2019GL083272>
- Hedin, J., Rapp, M., Khaplanov, M., Stegman, J., & Witt, G. (2012). Observations of NO in the upper mesosphere and lower thermosphere during ECOMA 2010. *Annales Geophysicae*, *30*(11), 1611–1621. <https://doi.org/10.5194/angeo-30-1611-2012>
- Liang, J., Donovan, E., Jackel, B., Spanswick, E., & Gillies, M. (2016). On the 630 nm red-line pulsating aurora: Red-line Emission Geospace Observatory observations and model simulations. *Journal of Geophysical Research: Space Physics*, *121*, 7988–8012. <https://doi.org/10.1002/2016JA022901>
- MacDonald, E. A., Donovan, E., Nishimura, Y., Case, N. A., Gillies, D. M., Gallardo-Lacourt, B., et al. (2018). New science in plain sight: Citizen Scientists lead to the discovery of optical structure in the upper atmosphere. *Science Advances*, *4*(3), eaaq0030. <https://doi.org/10.1126/sciadv.aqa0030>
- Mende, S. B., & Turner, C. (2019). Color ratios of subauroral (STEVE) arcs. *Journal of Geophysical Research: Space Physics*, *124*, 5945–5955. <https://doi.org/10.1029/2019JA026851>
- Nishimura, Y., Gallardo-Lacourt, B., Zou, Y., Mishin, E., Knudsen, D. J., Donovan, E. F., et al. (2019). Magnetospheric signatures of STEVE: Implication for the magnetospheric energy source and inter-hemispheric conjugacy. *Geophysical Research Letters*, *46*, 5637–5644. <https://doi.org/10.1029/2019GL082460>
- Rees, M. H., & Roble, R. G. (1975). Observations and theory of the formation of stable auroral red arcs. *Reviews of Geophysics*, *13*(1), 201–242. <https://doi.org/10.1029/RG013i001p00201>
- Sharp, W. E. (1984). On the temperature dependence of the reaction $O + NO \rightarrow NO_2$. *Planetary and Space Science*, *32*, 257–260.
- Solomon, S. C., Hays, P. B., & Abreu, V. J. (1988). The auroral 6300 Å emission: Observations and modeling. *Journal of Geophysical Research*, *93*(A9), 9867–9882. <https://doi.org/10.1029/JA093iA09p09867>
- Sternberg, J. R., & Ingham, M. F. (1972). Observations of the airglow continuum. *Monthly Notices of the Royal Astronomical Society*, *159*, 1–20.
- Unick, C. W., Donovan, E., Connors, M., & Jackel, B. (2017). A dedicated H-beta meridian scanning photometer for proton aurora measurement. *Journal of Geophysical Research: Space Physics*, *122*, 753–764. <https://doi.org/10.1002/2016JA022630>
- Zipf, E. C., Borst, W. L., & Donahue, T. M. (1970). A mass spectrometer observation of NO in an auroral arc. *Journal of Geophysical Research*, *75*(31), 6371–6376. <https://doi.org/10.1029/JA075i031p06371>